Engineering Analysis with Boundary Elements 74 (2017) 24–33

Contents lists available at ScienceDirect

Engineering Analysis with Boundary Elements

journal homepage: www.elsevier.com/locate/enganabound

BEM numerical simulation of coupled heat, air and moisture flow through a multilayered porous solid

L. Škerget[a,*], A. Tadeu[b], J. Ravnik[a]

[a] Faculty of Mechanical Engineering, University of Maribor, Smetanova 17, SI-2000 Maribor, Slovenia
[b] Department of Civil Engineering, University of Coimbra, Polo II, Rua Luis Reis Santos, 3030-788 Coimbra, Portugal

ARTICLE INFO

Keywords:
Heat
Air and moisture transport
Porous media
Boundary element method
Diffusion convection equation

ABSTRACT

The problem of unsteady coupled moisture, air and heat energy transport through a porous solid is studied numerically using singular boundary integral representation of the governing equations. The governing transport equations are written and solved for the continuous driving potentials, i.e. relative humidity, temperature and air pressure. The boundary and interface conditions are discussed.

The integral equations are discretized using mixed-boundary elements and a multidomain method also known as the macro-elements technique. The numerical model uses quadratic approximation over space and linear approximation over time for all field functions, which provides highly accurate numerical results. Three test benchmark examples (moisture uptake in a semi-infinite region, air transfer through a lightweight wall, and moisture redistribution inside a multilayered wall with capillary-active interior insulation), were analyzed to show the applicability and accuracy of the simulation model developed.

1. Introduction

Building envelopes are exposed simultaneously to indoor and outdoor climate changes. Differences in temperature, moisture and air pressure have a major impact on the sustainability of building components. It is highly important to develop reliable numerical simulation tools that can handle the coupled heat, air and moisture (HAM) phenomena and accurately capture the hygrothermal behavior of building components and their influence on the indoor environment. Many HAM numerical simulation models have been developed in recent years, based on a variety of discretization techniques for numerical approximation [15]. However, all these models require a reliable set of heat, air and moisture transport properties of porous materials [11].

This paper extends the work reported in an earlier paper [14], where only the coupling between the moisture and heat transport equations was performed. Only Dirichlet and Neumann boundary conditions were simulated then. In this paper, however, the coupling includes the airflow dynamic equation, and the transport moisture content discontinuous equation is replaced by the relative humidity continuous equation. In the new formulation, vapor mass and heat energy convection fluxes were simulated, and boundary conditions of the third or Cauchy type are also implemented.

In this paper, the three coupled transient HAM transport equations are solved using a boundary element numerical model (BEM). BEM is especially efficient at handling linear transport problems, where only the boundary of the solution domain has to be discretized. The scale of the problem is thus substantially reduced. Since the BEM numerical model is based on an inverse formulation, the field functions and their fluxes are computed with equal accuracy [9]. However, the domain discretization is required to capture nonlinear material effects. The singular integral representation is based on the use of an appropriate fundamental solution that incorporates some of the physics of the transport phenomenon, such as accumulation and diffusion of the field function. Accurate descriptions of the different time and length scales can be accommodated and treated much more reliably in a physically and mathematically justified manner. A serious drawback of the BEM is that it leads to a fully populated system of equations. However, this can be efficiently overcome by the subdomain or macro-element approach, which yields a sparse system similar to the domain type numerical models [7] while maintaining the accuracy and stability of the numerical algorithm. The discretization used in this paper leads to an overdetermined system of equations [12,13].

We next briefly set out the problem. The relevant governing differential equations for energy, moisture and air transport are considered and formulated for the continuous driving potentials, i.e. relative humidity, temperature and air pressure.

The mathematical description of the transport problems ends with

* Corresponding author at: Faculty of Mechanical Engineering, University of Maribor, Smetanova 17, SI-2000 Maribor, Slovenia.
E-mail addresses: leo@uni-mb.si (L. Škerget), tadeu@itecons.uc.pt (A. Tadeu), jure.ravnik@um.si (J. Ravnik).

http://dx.doi.org/10.1016/j.enganabound.2016.10.004
Received 14 December 2015; Accepted 3 October 2016
0955-7997/ © 2016 Elsevier Ltd. All rights reserved.

Nomenclature

c_{pm}	specific heat capacity of dry material, J/kg K
c_{pl}	specific heat capacity of liquid water, J/kg K
c_{pv}	specific heat capacity of water vapor, J/kg K
c_{pa}	specific heat capacity of air J/kg K
ρ_m	solid matrix density, kg/m^3
ρ_l	liquid water density, 1000 kg/m^3
ρ_v	density of water vapor, kg/m^3
λ	thermal conductivity, W/m K
δ_o	vapor permeability of still air, s
$\delta_p = \delta_o/\mu$	vapor permeability of material, s
μ	diffusion resistance factor, –
D_l	liquid permeability of material, s
δ_a	air permeability of material, s
k_l	liquid flow coefficient, m^2
k_l	air flow coefficient, m^2
ν_l	liquid water kinematic viscosity, m^2/s
ν_a	kinematic viscosity of air, m^2/s
D_{va}	vapor diffusivity in air, $26.1\cdot10^{-6}$ m^2/s
D_φ	moisture transport coefficient, kg/m s
$D_m = D_\varphi/\theta$	moisture diffusivity, m^2/s
D_T	moisture transport coefficient, kg/m s K
p_s	saturation pressure, Pa
p_l	pore liquid water pressure, Pa
p_v	water vapor pressure, Pa
T	temperature K, °C
W	moisture content, kg/m^3
$\varphi = p_v/p_s$	relative humidity, –
$\theta = dW/d\varphi$	sorption capacity, kg/m^3
Y_v	mass fraction of water vapor, –
Y_l	mass fraction of liquid water, –
j	moisture mass flux, kg/m^2 s
j_l	liquid water mass flux, kg/m^2 s
j_v	water vapor mass flux, kg/m^2 s
$\dot{m}_C$	moisture condensation rate, kg/m^3 s
R_w	water vapor gas constant, 461.4 J/kg K
R_a	air gas constant, J/kg K
M_w	water molecular mass, kg/kmol
β_p	vapor transfer coefficient, s/m
α	heat transfer coefficient, W/m^2 K

a discussion of the corresponding boundary and interface conditions. The related singular integral representations are then developed that describe the nonlinear heat, moisture and air transport in an integral form. The nonlinearity of the coupled diffusion–convection problem is handled by using an iterative solution strategy, based on an under-relaxation procedure. We give three benchmark test examples involving moisture uptake in a semi-infinite region, air transfer through a lightweight wall, and moisture redistribution inside a multilayered wall with capillary-active interior insulation to show the efficiency and accuracy of the proposed solution strategy [2,3].

2. Governing equations for a two-phase system

Let us consider a two-component, two-phase thermodynamic system in a solution domain Ω bounded by a control surface Γ, where the indices w, a and m represent the water, air and dry porous material, and the indices l and v represent the two water phases. That is, l refers to the liquid water and v to the vapor water in a liquid/vapor moisture system.

2.1. Moisture transport equation

The water moisture mass balance equation describing accumulation within the control volume, the moisture mass flux, e.g. diffusion/conduction and convection in and out of the control volume, and the generation of a species via phase change written for the water vapor and liquid water [1,2] is

$$\rho_m \frac{\partial Y_v}{\partial t} = -\vec{\nabla}\cdot\vec{n}_v - \dot{m}_C = -\vec{\nabla}\cdot(\vec{j}_v + \vec{j}_{v,conv}) - \dot{m}_C,\ \rho_m \frac{\partial Y_l}{\partial t} = -\vec{\nabla}\cdot\vec{j}_l + \dot{m}_C, \tag{1}$$

where the total vapor mass flux $\vec{n}_v$ combines the diffusion $\vec{j}_v$ and the convection $\vec{j}_{v,conv}$ driven parts, e.g. $\vec{n}_v = \vec{j}_v + \vec{j}_{v,conv}$, and the liquid mass flow considers only the conduction part $\vec{j}_l$. The dimensionless field functions $Y_v = m_v/m_m$ and $Y_l = m_l/m_m$ represent the mass fractions or moisture ratios of water vapor and liquid water, respectively, and m_m represents the mass of the dry porous material, whilst the quantities ρ_m, and $\dot{m}_C$ denote the mass density of the solid porous matrix and the moisture mass condensation/evaporation rate, respectively. The governing conservation equation for the moisture flow through a porous solid can now be derived by adding the individual species conservation equations (1), yielding

$$\frac{\partial W}{\partial t} = -\vec{\nabla}\cdot(\vec{j}_v + \vec{j}_{v,conv} + \vec{j}_l), \tag{2}$$

where the derived potential field function $W = \rho_m Y_v + \rho_m Y_l = m_w/V_m$ represents moisture content $m_w = m_v + m_l$ per volume of dry material V_m.

Using constitutive models to express the vapor diffusion mass flux $\vec{j}_v$, vapor convection mass flux $\vec{j}_{v,conv}$, and liquid conduction mass flux $\vec{j}_l$ due to the capillary suction and gravity effect, respectively, we can write

$$\vec{j}_v = -\delta_p \vec{\nabla} p_v,\quad \vec{j}_{v,conv} = \rho_m Y_v \vec{v} \quad \text{and} \quad \vec{j}_l = -D_l \vec{\nabla} p_l + D_l \rho_l \vec{g}, \tag{3}$$

where the driving potentials p_v and p_l are the vapor pressure and the pore liquid pressure, respectively, and the vector quantities $\vec{v}$ and $\vec{g}$ are the air velocity and the gravity acceleration. The transport coefficients $\delta_p = \delta_o/\mu$ and $D_l = k_l/\nu_l$ are the vapor and liquid permeability of the porous material, respectively, and the quantities δ_o, μ, k_l, ν_l and ρ_l represent the vapor diffusion in still air, the diffusion resistance factor, the liquid flow coefficient, the liquid water kinematic viscosity and the liquid water mass density.

Substituting the mass flux equations (3) into the conservation equation (2) gives the governing moisture transport equation due to water vapor diffusion and convection, liquid water conduction and gravity:

$$\frac{\partial W}{\partial t} = \vec{\nabla}\cdot(\delta_p \vec{\nabla} p_v - \rho_m Y_v \vec{v} + D_l \vec{\nabla} p_l - D_l \rho_l \vec{g}). \tag{4}$$

The moisture transport equation (4) consists of various moisture driving potentials, i.e. moisture content W, partial water vapor pressure p_v, the pore liquid pressure p_l and vapor mass ratio Y_v. Consequently, all terms in Eq. (4) have to be mathematically transformed using relative humidity φ and temperature T as primitive driving potentials. Using the following relations for the mass fluxes

$$\begin{aligned}
\vec{j}_v &= -\delta_p \vec{\nabla}(\varphi p_s) = -\delta_p p_s \vec{\nabla}\varphi - \delta_p \frac{dp_s}{dT}\vec{\nabla} T\varphi,\\
\vec{j}_{v,conv} &= \rho_m Y_v \vec{v} = \omega \vec{j}_{a,conv} = \omega\rho_a \vec{v} = \frac{1}{R_w}\frac{p_s}{T}\vec{v}\varphi,\\
\vec{j}_l &= -D_l \vec{\nabla}(R_w T \rho_l \ln(\varphi)) + D_l \rho_l \vec{g} = -D_l R_w \rho_l \frac{T}{\varphi}\vec{\nabla}\varphi - D_l R_w \rho_l \ln(\varphi)\vec{\nabla} T\\
&\quad + D_l \rho_l \vec{g},
\end{aligned} \tag{5}$$

where the quantities $\vec{j}_{a,conv} = \rho_a \vec{v}$, ω and $p_s(T)$ are the air convection mass flux, the absolute humidity and the saturation pressure, respec-

tively, and R_w and ρ_a are the water vapor gas constant and the air mass density, the following moisture transport equation can be formulated:

$$\theta\frac{\partial\varphi}{\partial t} = \vec{\nabla}\cdot\left(D_\varphi\vec{\nabla}\varphi + D_T\vec{\nabla}T - \frac{1}{R_w}\frac{p_s}{T}\vec{v}\varphi - D_l\rho_l\vec{g}\right), \tag{6}$$

where $\theta = dW/d\varphi$ is the slope of the sorption isotherm $W = W(\varphi)$. The primitive variable in Eq. (6) is the relative humidity field function $\varphi(r_j, t)$, whilst the second, third and fourth terms on the right side of the equation act as homogeneous nonlinear source terms due to temperature gradient, vapor convection and gravity force. Note that, due to the second and third terms, Eq. (6) is explicitly coupled to the heat energy transport equation and pressure equation. The transport coefficients D_φ and D_T are given as:

$$D_\varphi = \delta_p p_s + D_l R_w \rho_l \frac{T}{\varphi} \quad \text{and} \quad D_T = \delta_p \frac{dp_s}{dT}\varphi + D_l R_w \rho_l \ln(\varphi). \tag{7}$$

2.2. Heat energy transport equation

The heat energy balance equation considers accumulation within the control volume, energy flux (sensitive, latent and convective), in and out of the control volume and heat source/sink term [1–3], as follows:

$$\rho_m c_{p,eff}\frac{\partial T}{\partial t} = -\vec{\nabla}\cdot\vec{q} + I = -\vec{\nabla}\cdot(\vec{q}_{sens} + \vec{q}_{lat} + \vec{q}_{conv}) + I, \tag{8}$$

where the specific capacities per mass $c_{p,eff} = c_{pm} + c_{pl}W/\rho_m$, c_{pm} and c_{pl} refer to the effective, dry porous material and to liquid water, I denotes a heat source per unit volume, and the sensible heat energy flux $\vec{q}_{sens}$, the latent heat flux $\vec{q}_{lat}$ and the convective heat flux $\vec{q}_{conv} = \vec{q}_{a,conv} + \vec{q}_{v,conv}$, due to air and vapor convection, are

$$\begin{aligned}
&\vec{q}_{sens} = -\lambda_{eff}\vec{\nabla}T,\\
&\vec{q}_{lat} = h_{lat}\vec{n}_v = [h_e + (c_{pv} - c_{pl})T](\vec{j}_v + \vec{j}_{v,conv}) = -h_{lat}(\delta_p\vec{\nabla}p_v - \omega\rho_a\vec{v}),\\
&\vec{q}_{conv} = \vec{q}_{a,conv} + \vec{q}_{v,conv} = c_{pa}T\vec{j}_{a,conv} + c_{pv}T\vec{j}_{v,conv} = \rho_a(c_{pa} + \omega c_{pv})\vec{v}T,
\end{aligned} \tag{9}$$

where h_{lat} denotes specific latent enthalpy, h_e is specific latent enthalpy of evaporation or condensation and the quantities c_{pv}, c_{pa} and λ_{eff} denote the specific heat per mass of water vapor, the specific heat per mass of air and effective thermal conductivity, respectively. Substituting heat flux equations (9) into conservation equation (8) gives

$$c_{eff}\frac{\partial T}{\partial t} = \vec{\nabla}\cdot[\lambda_{eff}\vec{\nabla}T - h_{lat}\vec{n}_v - \rho_a(c_{pa} + \omega c_{pv})\vec{v}\,T] + I, \tag{10}$$

where the primitive variable in Eq. (10) is the temperature field $T(r_j, t)$, whilst the coefficient $c_{eff} = \rho_m c_{p,eff}$ is the effective specific heat per unit volume.

2.3. Airflow dynamic equations

The primitive field functions of interest for the airflow through a porous solid are the velocity vector field $v_i(r_j, t)$ and the scalar pressure field $p(r_j, t)$, so that the mass and momentum equations are given by

$$\frac{\partial}{\partial x_j}(\rho_a v_j) = 0, \tag{11}$$

$$\rho_a v_j = -\delta_a\frac{\partial p}{\partial x_j}, \tag{12}$$

where the quantities $\delta_a = k_a/\nu_a$, k_a and ν_a represent the air permeability, the airflow coefficient and the air kinematic viscosity, respectively.

The pressure equation is derived by applying the *div* operator to Eq. (12), resulting in the elliptic Poisson pressure equation

$$\frac{\partial}{\partial x_j}\left(\delta_a\frac{\partial p}{\partial x_j}\right) = 0, \tag{13}$$

where the time dependence of the two field functions, velocity and pressure, account for the effect of time-dependent pressure boundary conditions.

2.4. Initial and boundary conditions

To close the mathematical model governing the heat, moisture and air time dependent transport in a porous material we need to know the initial and boundary conditions for the relative humidity φ, temperature T and air pressure p.

The initial conditions in general represent the distribution of field functions in the solution domain and their normal derivatives on the boundary and are given by the following relations:

$$\begin{aligned}
&\varphi = \overline{\varphi}, \quad T = \overline{T} \quad \text{and} \quad p = \overline{p} \quad \text{in } \Omega \text{ at } t = t_o,\\
&\frac{\partial\varphi}{\partial n} = \frac{\overline{\partial\varphi}}{\partial n} \quad \text{and} \quad \frac{\partial T}{\partial n} = \frac{\overline{\partial T}}{\partial n} \quad \text{on } \Gamma \text{ for } t = t_o.
\end{aligned} \tag{14}$$

As a rule, the heat and moisture exchange between a solid wall surface and its surrounding medium can be prescribed by the boundary conditions of the first, second and third kinds on the parts of the boundary Γ_1, Γ_2 and Γ_3, respectively, such that the solution boundary $\Gamma = \Gamma_1 + \Gamma_2 + \Gamma_3$.

The boundary conditions of the first or Dirichlet kind, where surface conditions are the same as the ambient conditions, are given by the known surface value of the driving potentials:

$$T = \overline{T} \quad \text{and} \quad \varphi = \overline{\varphi} \quad \text{on } \Gamma_1 \text{ for } t > t_o, \tag{15}$$

and this condition can be applied when the building component is in contact with water or earth. In the case of liquid transport, this applies when the component surface is completely wetted by rain or ground water.

Boundary conditions of the second or Neumann type require knowledge of heat or mass flow at the surface and are given by the prescribed surface temperature and relative humidity normal derivative values, respectively:

$$\frac{\overline{\partial T}}{\partial n} = -\frac{q_{sens}}{\lambda_{eff}} \quad \text{and} \quad \frac{\overline{\partial\varphi}}{\partial n} = -\frac{j_v}{\delta_p p_s} - \frac{dp_s}{dT}\frac{\varphi}{p_s}\frac{\partial T}{\partial n} \quad \text{on } \Gamma_2 \text{ for } t > t_o. \tag{16}$$

Symmetry conditions and adiabatic or moisture-tight conditions are given by the zero flux condition, i.e. $\partial T/\partial n = \partial\varphi/\partial n = 0$.

Boundary conditions of the third or Cauchy type are the most common kind of heat and moisture transfer between the component surface and the ambient. Special compatibility and restriction conditions must be satisfied at the boundary surfaces of the heat and moisture transfer region. There must be an energy and moisture balance between the heat/moisture flow within the solid to/from the surface, and the heat/moisture that is leaving/entering the surface.

Let us first consider vapor transfer. The normal total vapor flux $n_v = \vec{n}_v\cdot\vec{n} = (\vec{j}_v + \vec{j}_{v,conv})\cdot\vec{n}$ flowing within the solid from the surface must be equal to the vapor transfer from the ambient, denoted by the index a, to the solid surface given by the constitutive model as follows:

$$-n_v = \delta_p\frac{\partial p_v}{\partial n} - j_{v,conv} = \beta_p(p_{v,a} - p_v) - j_{v,conv,a} \quad \text{on } \Gamma_3 \text{ for } t > t_o, \tag{17}$$

where the quantities β_p and $p_{v,a}$ are the vapor transfer coefficient and ambient vapor pressure, respectively. Eq. (17) can be transformed using relative humidity and the temperature as driving potentials as follows:

$$-n_v = \delta_p p_s\frac{\partial\varphi}{\partial n} + \delta_p\frac{dp_s}{dT}\frac{\partial T}{\partial n}\varphi - j_{v,conv} = \beta_p(p_{v,a} - \varphi p_s) - j_{v,conv,a}, \tag{18}$$

yielding an expression for the relative humidity normal derivative

$$\frac{\partial\varphi}{\partial n} = -\left(\frac{\beta_p}{\delta_p} + \frac{1}{p_s}\frac{dp_s}{dT}\frac{\partial T}{\partial n}\right)\varphi + \frac{\beta_p}{\delta_p}\frac{p_{v,a}}{p_s} + \frac{1}{\delta_p p_s}(j_{v,conv} - j_{v,conv,a}). \tag{19}$$

Based on Eq. (19) we can conclude that vapor convective fluxes canceled each other out in all outflow surfaces, $j_{v,conv} = j_{v,conv,a}$.

Heat transfer can be treated in the same way. The normal total heat flux $q = \vec{q}\cdot\vec{n} = (\vec{q}_{sens} + \vec{q}_{lat} + \vec{q}_{conv})\cdot\vec{n}$ flowing within the solid from the surface must be equal to the heat inflow from the ambient to the solid surface given by the following constitutive model:

$$-q = \alpha(T_a - T) - h_{lat,a}n_v - q_{conv,a} + q_{sol} \quad \text{on } \Gamma_3 \text{ for } t > t_o, \tag{20}$$

where the ambient temperature is denoted by T_a and the heat transfer coefficient is given by summing the convective and radiation parts $\alpha = \alpha_{con} + \alpha_{rad}$. The term q_{sol} represents heat flow from short-wave solar radiation. Substituting Eqs. (9) for the sensible heat flow into Eq. (20) gives

$$-q = \lambda_{eff}\frac{\partial T}{\partial n} - h_{lat}n_v - q_{conv} = \alpha(T_a - T) - h_{lat,a}n_v - q_{conv,a} + q_{sol}, \tag{21}$$

yielding an expression for the temperature normal derivative:

$$\frac{\partial T}{\partial n} = \frac{\alpha}{\lambda_{eff}}(T_a - T) + \frac{1}{\lambda_{eff}}[q_{sol} + (h_{lat} - h_{lat,a})n_v + (q_{conv} - q_{conv,a})]. \tag{22}$$

Again, we can conclude, that the latent and convective fluxes canceled each other out at all outflow boundaries.

The Dirichlet and Neumann boundary conditions for the pressure equation can be determined for the solution boundary and the following relations are valid:

$$p = \overline{p} \ \text{ on } \Gamma_1 \quad \text{and} \quad \frac{\partial p}{\partial n} = \frac{\overline{\partial p}}{\partial n} = -\frac{\rho_a}{\delta_a}v_n \ \text{ on } \Gamma_2, \tag{23}$$

where $v_n = \vec{v}\cdot\vec{n}$ is the normal velocity component.

2.5. Interface conditions

When simulating conservation problems for an arbitrary field function $u(\vec{r}, t)$, we encounter transport problems such as heat, moisture and momentum transfer between two adjacent media/macro-elements labeled 1 and 2. In the equilibrium state, the individual driving potentials, i.e. temperature, relative humidity or air pressure, denoted by $u^{(1)}$ and $u^{(2)}$, satisfy the governing transport equation. At the interface, denoted by Γ_I, the physical considerations provide us with the necessary expressions for the compatibility and equilibrium conditions.

The chosen driving potentials for heat and moisture transport in porous media, the relative humidity φ, the vapor pressure p_v and temperature T are continuous field functions at the contact between the two porous materials, therefore the compatibility conditions give us the equalities:

$$T^{(1)} \equiv T^{(2)} \equiv T^{(I)} \quad \text{and} \quad \varphi^{(1)} \equiv \varphi^{(2)} \equiv \varphi^{(I)} \quad \text{on } \Gamma_I. \tag{24}$$

The energy and moisture equilibrium conditions at the interface Γ_I between Ω_1 and Ω_2 are given by continuous energy flow $\vec{q} = \vec{q}_{sens} + \vec{q}_{lat}$ and continuous moisture flow $\vec{j} = \vec{j}_v + \vec{j}_l$ across the interface, respectively. The energy equilibrium conditions across the interface can therefore be stated as:

$$(\vec{q}_{sens} + \vec{q}_{lat})^{(1)}\cdot\vec{n}^{(1)} \equiv -(\vec{q}_{sens} + \vec{q}_{lat})^{(2)}\cdot\vec{n}^{(2)} \quad \text{on } \Gamma_I, \tag{25}$$

or, in the extended form for the temperature normal derivative $(\partial T/\partial n)^{(2)}$:

$$\left(\frac{\partial T}{\partial n}\right)^{(2)} = -\frac{\lambda_{eff}^{(1)}}{\lambda_{eff}^{(2)}}\left(\frac{\partial T}{\partial n}\right)^{(1)} + \frac{1}{\lambda_{eff}^{(2)}}[(\vec{q}_{lat}\cdot\vec{n})^{(1)} + (\vec{q}_{lat}\cdot\vec{n})^{(2)}] \tag{26}$$

and the moisture equilibrium conditions across the interface can likewise be written as:

$$(\vec{j}_v + \vec{j}_l)^{(1)}\cdot\vec{n}^{(1)} \equiv -(\vec{j}_v + \vec{j}_l)^{(2)}\cdot\vec{n}^{(2)} \quad \text{on } \Gamma_I, \tag{27}$$

or, in extended expression for the relative humidity normal derivative

$$\left(\frac{\partial\varphi}{\partial n}\right)^{(2)} = -\frac{D_\varphi^{(1)}}{D_\varphi^{(2)}}\left(\frac{\partial\varphi}{\partial n}\right)^{(1)} - \frac{1}{D_\varphi^{(2)}}\left[\left(D_T\frac{\partial T}{\partial n}\right)^{(1)} + \left(D_T\frac{\partial T}{\partial n}\right)^{(2)}\right]. \tag{28}$$

The air flow interface conditions can be given by the following compatibility and equilibrium conditions:

$$p^{(1)} \equiv p^{(2)} \equiv p^{(I)} \quad \text{and} \quad \delta_a^{(1)}\left(\frac{\partial p}{\partial n}\right)^{(1)} \equiv -\delta_a^{(2)}\left(\frac{\partial p}{\partial n}\right)^{(2)} \quad \text{on } \Gamma_I. \tag{29}$$

3. Boundary element numerical model

3.1. Integral representation for energy and moisture transport equations

The mathematical model described above is solved with a boundary element method approach. The boundary-domain integral equations are integrated over an elementary subdomain/macro-element. The unique property that gives the boundary element method an advantage over other domain type numerical techniques is its use of Green's fundamental solutions as particular weighting functions [8,9]. Since the fundamental solutions only consider the linear transport phenomenon, the appropriate selection of a linear differential operator $L[\,\cdot\,]$ is of crucial importance when establishing a stable and accurate singular integral representation that corresponds to the original differential conservation equation.

The differential energy and moisture conservation models written for the primitive field function temperature and relative humidity, respectively, can be written in the following general form [7]:

$$L[\,u\,] + \frac{\partial b_j}{\partial x_j} + b = a_o\frac{\partial u^2}{\partial x_j\partial x_j} - \frac{\partial u}{\partial t} + \frac{\partial b_j}{\partial x_j} + b = 0, \tag{30}$$

where the notation $L[\,\cdot\,]$ stands for the parabolic diffusion linear operator, $u(r_j, t)$ is an arbitrary field function, and the terms $b_j(r_j, t)$ and $b(r_j, t)$ represent inhomogeneous or source effects due to the nonlinear transport coefficients, convection and production of the conservative field function, respectively, with the following corresponding integral representation [6] written for a time step $\Delta t = t_F - t_{F-1}$:

$$\begin{aligned} c(\xi)u(\xi, t_F) + a_o\int_\Gamma\int_{t_{F-1}}^{t_F} uq^\star dtd\Gamma = {} & \int_\Gamma\int_{t_{F-1}}^{t_F}(a_o q_j + b_j)n_j u^\star dtd\Gamma \\ & - \int_\Omega\int_{t_{F-1}}^{t_F} b_j q_j^\star dtd\Omega + \int_\Omega\int_{t_{F-1}}^{t_F} bu^\star dtd\Omega \\ & + \int_\Omega u_{i,F-1}u_{F-1}^\star d\Omega, \end{aligned} \tag{31}$$

where $q = \partial u/\partial n = q_j n_j$ and $u^\star(\xi, s; t_F, t)$ are the field function normal flux and the parabolic diffusion fundamental solution [8], respectively, where s is an arbitrary field point in the solution domain or on the boundary, and ξ is the source point. The nonhomogeneous terms b_j and b are given by the following relations, i.e. for the energy transport:

$$b_j = \frac{1}{c_o}\left[\tilde{\lambda}\frac{\partial T}{\partial x_j} - h_{lat}n_{vj} - \left(\rho_a c_{pa} + \frac{c_{pv}}{R_w}\frac{p_s}{T}\varphi\right)v_j T\right], \quad b = -\frac{\tilde{c}}{c_o}\frac{\partial T}{\partial t} + \frac{I}{c_o}, \tag{32}$$

with $c_{eff} = c_o + \tilde{c}$, $\lambda_{eff} = \lambda_o + \tilde{\lambda}$ and $a_o = \lambda_o/c_o$, and for the moisture transport:

$$b_j = \frac{1}{\theta_o}\left(\widetilde{D_\varphi}\frac{\partial\varphi}{\partial x_j} + D_T\frac{\partial T}{\partial x_j} - D_l\rho_l g_j - \frac{1}{R_w}\frac{p_s}{T}v_j\varphi\right), \quad b = -\frac{\tilde{\theta}}{\theta_o}\frac{\partial\varphi}{\partial t}, \tag{33}$$

and $\theta = \theta_o + \widetilde{\theta}$, $D_\varphi = D_{\varphi,o} + \widetilde{D_\varphi}$ and $a_o = D_{m,o} = D_{\varphi,o}/\theta_o$.

3.2. Integral representation for air dynamics

Employing the linear elliptic Laplace differential operator, the following relation may be considered for the pressure equation (23):

$$L[\,p\,] + \frac{\partial b_j}{\partial x_j} = \frac{\partial^2 p}{\partial x_j \partial x_j} + \frac{\partial b_j}{\partial x_j} = 0, \tag{34}$$

with the corresponding boundary-domain integral representation:

$$c(\xi)p(\xi) + \int_\Gamma pq^\star d\Gamma = \int_\Gamma \frac{\partial p}{\partial n} u^\star d\Gamma + \int_\Gamma b_j n_j u^\star d\Gamma - \int_\Omega b_j q_j^\star d\Omega, \tag{35}$$

where $u^\star(\xi, s)$ is the elliptic Laplace fundamental solution [9], whilst the inhomogeneous nonlinear term b_j is given by the following expression:

$$b_j = \frac{\widetilde{\delta_a}}{\delta_{ao}} \frac{\partial p}{\partial x_j}, \tag{36}$$

and $\delta_a = \delta_{ao} + \widetilde{\delta_a}$. For the constant air permeability δ_a, the pseudo-force term $b_j \equiv 0$, and the pressure field is given by the linear Laplace equation represented by the first two boundary integrals in Eq. (35).

3.3. Discretized equations

For the numerical solution of Eq. (31), the boundary Γ is discretized into a series of boundary elements and the domain Ω is discretized into a series of internal cells. Furthermore, field functions and their derivatives are assumed to vary within each element or cell and each time step, according to the space $\{\Phi\}$ or $\{\phi\}$ and time $\{\Psi\}$ interpolation functions such that

$$\begin{aligned} u(S,t) &= \{\Phi\}^T\{\Psi\}\{u\}_m^n, \quad q(S,t) = \{\Phi\}^T\{\Psi\}\{q\}_m^n, \\ b_j(S,t) &= \{\Phi\}^T\{\Psi\}\{b_j\}_m^n, \quad b_j(s,t) = \{\phi\}^T\{\Psi\}\{b_j\}_m^n, \text{ etc.}, \end{aligned} \tag{37}$$

where index n refers to the number of nodes within each element or cell, and the index m refers to the degree of variation of the function $\{\Psi\}$. Assuming linear variation of all functions within the individual time increment $\tau = t_F - t_{F-1}$, i.e. m=1,2 and

$$\Psi_1 = \frac{t_F - t}{\tau} \quad \text{and} \quad \Psi_2 = \frac{t - t_{F-1}}{\tau}, \tag{38}$$

the analytical expressions for the time integrals

$$U_m^\star = a_o \int_{t_{F-1}}^{t_F} \Psi_m u^\star dt, \quad Q_m^\star = a_o \int_{t_{F-1}}^{t_F} \Psi_m q^\star dt, \tag{39}$$

can be derived [14] and Eq. (31) can be rewritten as

$$\begin{aligned} c(\xi)u_2(\xi) + &\sum_{m=1}^{2}\sum_{e=1}^{E}\left[\int_{\Gamma_e}\{\Phi\}^T Q_m^\star d\Gamma\right]\{u\}_m^n \\ = &\sum_{m=1}^{2}\sum_{e=1}^{E}\left[\int_{\Gamma_e}\{\Phi\}^T U_m^\star d\Gamma\right]\{q\}_m^n + \sum_{m=1}^{2}\sum_{e=1}^{E}\left[\int_{\Gamma_e}\{\Phi\}^T U_m^\star n_j d\Gamma\right]\{\frac{b_j}{a_o}\}_m^n \\ &- \sum_{m=1}^{2}\sum_{c=1}^{C}\left[\int_{\Omega_c}\{\Phi\}^T Q_{jm}^\star d\Omega\right]\{\frac{b_j}{a_o}\}_m^n + \sum_{m=1}^{2}\sum_{c=1}^{C}\left[\int_{\Omega_c}\{\Phi\}^T U_m^\star d\Omega\right] \\ &\{\frac{b}{a_o}\}_m^n + \sum_{c=1}^{C}\left[\int_{\Omega_c}\{\Phi\}^T u_{F-1}^\star d\Omega\right]\{u\}_{F-1}^n, \end{aligned} \tag{40}$$

where the symbols E and C denote the number of boundary elements and internal cells, respectively. The above boundary and domain integrals, which are functions of geometry, the time step and material properties can be discretized as follows:

$$\begin{aligned} h_{em}^n &= \int_{\Gamma_e}\{\Phi\}^T Q_m^\star d\Gamma, \quad g_{em}^n = \int_{\Gamma_e}\{\Phi\}^T U_m^\star d\Gamma, \\ c_{ejm}^n &= \int_{\Gamma_e}\{\Phi\}^T U_m^\star n_j d\Gamma, \; d_{cm} = \int_{\Omega_c}\{\phi\}^T U_m^\star d\Omega, \\ d_{cjm} &= \int_{\Omega_c}\{\phi\}^T Q_{jm}^\star d\Omega, \quad b_c = \int_{\Omega_c}\{\phi\}^T u_{F-1}^\star d\Omega, \end{aligned} \tag{41}$$

yielding the following discretized form of Eq. (40):

$$\begin{aligned} c(\xi)u_2(\xi) + \sum_{m=1}^{2}\sum_{e=1}^{E}\{h\}_m^T\{u\}_m^n = &\sum_{m=1}^{2}\sum_{e=1}^{E}\{g\}_m^T\{q\}_m^n + \sum_{m=1}^{2}\sum_{e=1}^{E}\{c_j\}_m^u\{\frac{b_j}{a_o}\}_m^n \\ &- \sum_{m=1}^{2}\sum_{c=1}^{C}\{d_j\}_m^T\{\frac{b_j}{a_o}\}_m^n \\ &+ \sum_{m=1}^{2}\sum_{c=1}^{C}\{d\}_m^T\left\{\frac{b}{a_o}\right\}_m^n + \sum_{c=1}^{C}\{b\}^T\{T\}_1^n. \end{aligned} \tag{42}$$

Using the collocation method to apply the above statement to all boundary and domain nodes, and applying the notation, i.e. $[H] = [c(\xi)] + [\widehat{H}]$ and $[E_j] = [C_j] - [D_j]$, we get a nonlinear system of equations:

$$\begin{aligned} [H]_2\{u\}_2 + [H]_1\{u\}_1 = [G]_2\{q\}_2 + [G]_1\{q\}_1 + [E_j]_2\left\{\frac{b_j}{a_o}\right\}_2 + [E_j]_1\left\{\frac{b_j}{a_o}\right\}_1 \\ + [D]_2\left\{\frac{b}{a_o}\right\}_2 + [D]_1\left\{\frac{b}{a_o}\right\}_1 + [B]\{u\}_1. \end{aligned} \tag{43}$$

Based on the procedure developed for the energy and moisture transport equations, integral representation of the pressure Eq. (35) can be given in the following discretized form:

$$[H]\{p\} = [G]\left\{\frac{\partial p}{\partial n}\right\} + [E_j]\{b_j\}. \tag{44}$$

4. Numerical algorithm

When dealing with nonlinear transport problems the subdomain technique must be used to apply different constant diffusivity to each subdomain. The second reason for applying the subdomain or multi-domain model is to cut the storage and CPU time requirements of the single domain BEM approach [5,7,14]. The heat energy, moisture and pressure equations represent a coupled nonlinear system of equations that can only be solved iteratively. The nonlinear iterative solution algorithm is as follows:

- begin time step-loop
- begin global nonlinear loop
  1. calculate integrals for the energy and moisture kinetics
  2. *air flow dynamics, pressure equation*
     1. solve discretized equation (44) for pressure
     2. compute velocity field based on Eq. (12)
  3. *heat energy kinetics*
     1. begin local heat energy nonlinear loop

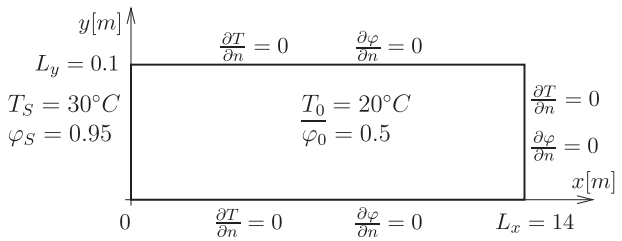

Fig. 1. A semi-infinite homogeneous structure: geometry, boundary and initial conditions.

Table 1
Parameters for all given materials [11,15,16].

Parameter	Brick (*A*)	Mortar (*B*)	Insulation (*C*)	Material (*D*)
Water retention				
W_{sat} (kg/m^3)	373.5	700.0	871.0	146.0
k_1 (–)	0.46	0.2	0.41	1.0
k_2 (–)	0.54	0.8	0.59	–
a_1(1/m)	0.47	0.5	0.006	$0.7848\cdot10^{-6}$
a_2 (1/m)	0.20	0.004	0.012	–
n_1 (–)	1.5	1.5	2.5	1.6
n_2 (–)	3.8	3.8	2.4	–
Vapor diffusion				
μ (–)	7.5	50.0	5.6	200.0
p (–)	0.20	0.20	0.20	0.497
Liquid conduction				
a_0 (–)	−36.484	−40.425	−46.245	−39.2619
a_1 (–)	+461.325	+83.319	+294.506	+0.0704
a_2 (–)	−5240.0	−175.961	−1439.0	$-1.7420\cdot10^{-4}$
a_3 (–)	$+2.907\cdot10^{+4}$	+123.863	+3249.0	$-2.7952\cdot10^{-6}$
a_4 (–)	$-7.41\cdot10^{+4}$	0	−3370.0	$-1.1566\cdot10^{-7}$
a_5 (–)	$+6.997\cdot10^{+4}$	0	+1305.0	$+2.5969\cdot10^{-9}$
Thermal conduction				
λ_m (W/m K)	0.682	0.6	0.06	1.5
λ_{mst} (W/m K)	0	0.56	0.56	15.8
Heat capacity				
ρ_m (kg/m^3)	1600.0	230.0	212.0	2280.0
c_{pm} (J/kg K)	1000.0	920.0	1000.0	800.0

1. solve discretized equation (43) for energy
2. use under-relaxation for computing new domain values
3. check convergence – local loop

2. end local heat energy loop

4. *moisture kinetics*
1. begin local moisture transport nonlinear loop
1. solve discretized equation (43) for moisture
2. use under-relaxation for computing new domain values
3. check convergence – local loop

2. end local moisture transport loop

5. *nonlinear effects* – calculate all nonlinear terms
1. use under-relaxation for computing new values

6. *check convergence*– global loop
7. end global nonlinear loop

- end time step loop

5. Numerical examples

Three one-dimensional benchmarks [3,15,16] were solved in 2D plane geometry. The benchmarks presented cover coupled heat, moisture and air transfer.

5.1. Moisture uptake within a semi-infinite region

The benchmark test example, shown in Fig. 1, was a single homogeneous material marked with (*D*) in Table 1 $L_x = 14.0\,m$ long and $L_y = 0.1\,m$ wide, in equilibrium with a constant surrounding environment [3]. The material was perfectly air tight. At a certain moment the temperature and the relative humidity underwent a step-change. A non-uniform non-symmetric mesh of $M = 400 \times 1R_x80$ macro-elements was used, with aspect ratio R_x=80 between the largest and the smallest boundary elements. The convergence criterion selected was $\epsilon = 10^{-9}$, and the under-relaxation parameter was set to *ur*=0.8. The time-dependent analysis was performed by running the simulation from the initial state with a time step value of $\Delta t = 1.0$ day and $\Delta t = 0.1$ day.

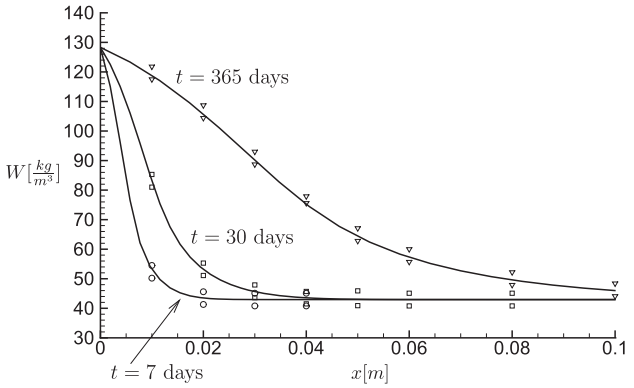

Fig. 2. Moisture field – time step $\Delta t = 1.0$ day: instantaneous results at the specific time instants, t = 7, 30 and 365 days; ○, □, ▽– limits of validity for numerical results [3].

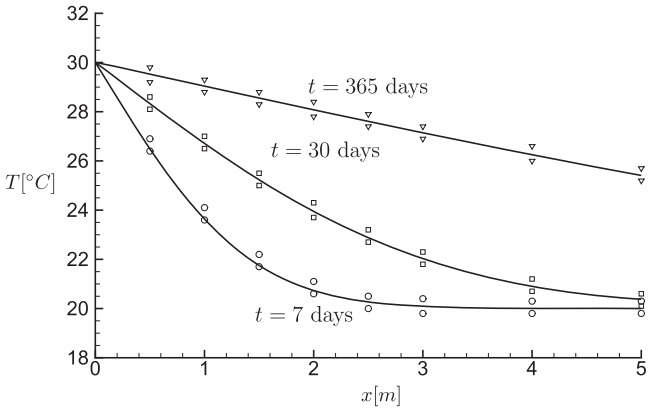

Fig. 3. Temperature field – time step $\Delta t = 1.0$ day: instantaneous results at the specific time instants, t = 7, 30 and 365 days; ○, □, ▽– limits of validity for numerical results [3].

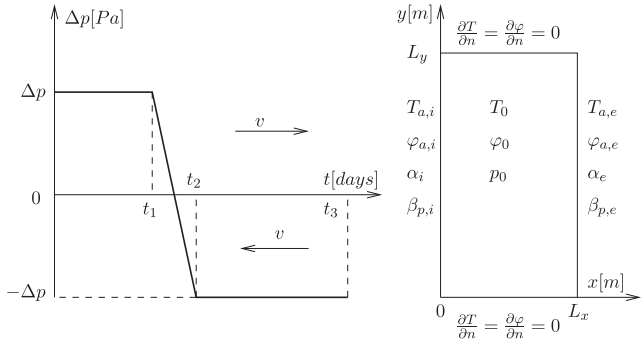

Fig. 4. Air flow through a lightweight wall: outline of the structure, initial and boundary conditions: L_x = 0.2 m, L_y = 0.002 m, t_1 = 20 days, t_2 = 21 days, t_3 = 100 days, Δp = 30 Pa.

The objective was to calculate the moisture and temperature distribution after t = 7, 30 and 365 days. The initial hygrothermal conditions of the structure were temperature T_o = 20 °C and relative humidity $\varphi_o = 0.50$. After the step change, the left surface of the structure was exposed to $\varphi_S = 0.95$ relative humidity and temperature T_S = 30 °C, whilst on the right surface the normal derivatives of the corresponding field functions were assumed to be zero. Therefore, the following boundary conditions of the first kind could be prescribed on the left boundary at *x*=0:

$$\varphi_S = 0.95 \quad \text{and} \quad T_S = 30\ ^\circ\text{C} \quad \text{on } x = 0 \text{ and } 0 \le y \le L_y \text{ for } t > 0, \tag{45}$$

and zero Neumann boundary conditions were prescribed elsewhere,

$$\frac{\partial \varphi}{\partial n} = 0 \quad \text{and} \quad \frac{\partial T}{\partial n} = 0 \quad \text{for } t > 0. \tag{46}$$

The initial conditions were

$$\varphi_o = 0.5 \quad \text{and} \quad T_o = 20\ ^\circ\text{C} \quad \text{at } t = 0. \tag{47}$$

The sorption isotherm was given by the following expression [3]:

$$W(\varphi) = W_{sat}\frac{k_1}{[1 + (a_1 h)^{n_1}]^{m_1}}, \quad h = \frac{p_{suc}}{\rho_l g} = -\frac{R_w T \ln(\varphi)}{g}, \tag{48}$$

with the exponent $m_1 = 1 - 1/n_1$. The vapor permeability δ_P and liquid water permeability D_l transport coefficients were given by the following expressions [3]:

$$\delta_p(W, T) = \frac{D_{va}}{\mu R_w T}\frac{1 - \frac{W}{W_{sat}}}{(1-p)\left(1 - \frac{W}{W_{sat}}\right)^2 + p}, \tag{49}$$

$$D_l(W) = \exp\left[\sum_{i=0}^{5} a_i (W - 73)^i\right]. \tag{50}$$

Effective thermal conductivity λ_{eff} and specific heat per volume for dry material c_m, respectively, were given by the following relationships [3]:

$$\lambda_{eff} = \lambda_m + \lambda_{mst}\frac{W}{\rho_l} \quad \text{and} \quad c_m = c_{pm}\rho_m. \tag{51}$$

All the relevant material parameters are given in Table 1 for the material (*D*).

Since there is practically no difference between simulation results for the time increment $\Delta t = 1.0$ day and the time increment $\Delta t = 0.1$ day, only the moisture and temperature distributions for the time increment $\Delta t = 1.0$ day are plotted in Figs. 2 and 3. As these figures show, the simulation model produced excellent results with a high degree of agreement with the benchmark solution presented in [3].

5.2. Air flow through a light weight wall

The benchmark test example [15,16] shown in Fig. 4 deals with the air transfer caused by a drop in air pressure $\Delta p = 30$ Pa through a single homogeneous material (*C*) layer $L_x = 0.2$ m thick and $L_y = 0.002$ m in height. Moisture transfer is caused mainly by air flow, but moisture and temperature gradients across the porous layer play a part, too. The simulation time is 100 days. There is air exfiltration in the first 20 days, which then changes to air infiltration. A non-uniform symmetric mesh of $M = 24 \times 1R_x2$ macro-elements was applied, with aspect ratio R_x=2 between the largest and the smallest boundary element. The convergence criterion selected was $\epsilon = 10^{-10}$, and the under-relaxation parameter was set to *ur*=0.001 to provide the convergent solution. The time-dependent analysis was performed by running the simulation from the initial state with a time step of $\Delta t = 1.00$ day and $\Delta t = 0.50$ day.

The initial hygrothermal conditions of the structure were temperature $T_o = 20\ ^\circ$C, relative humidity $\varphi_o = 0.95$ and air pressure $1.0 \cdot 10^5$ Pa. The following boundary conditions of the third kind could be prescribed on the left boundary at $x = 0$ m and $0 \le y \le L_y$,

$$T_{a,i} = 20.0\ ^\circ\text{C} \quad \text{and} \quad \alpha_i = 10.00\ \text{W/m}^2\,\text{K} \quad \text{for } t > 0 \varphi_{a,i} = 0.7 \quad \text{and} \quad \beta_{p,i} = 7.38 \cdot 10^{-12}\ \text{s/m} \quad \text{for } t > 0, \tag{52}$$

on the right boundary at $x = L_x$ and $0 \le y \le L_y$

$$T_{a,e} = 2.0\ ^\circ\text{C} \quad \text{and} \quad \alpha_e = 10.00\ \text{W/m}^2\,\text{K} \quad \text{for } t > 0 \varphi_{a,e} = 0.8 \quad \text{and} \quad \beta_{p,e} = 2.00 \cdot 10^{-7}\ \text{s/m} \quad \text{for } t > 0, \tag{53}$$

and zero boundary conditions of the second kind were prescribed elsewhere,

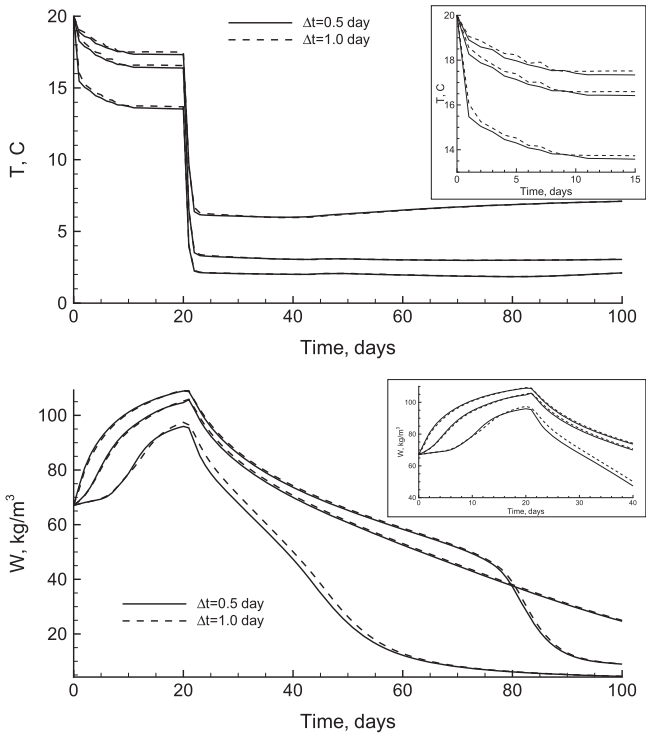

Fig. 5. Temperature and moisture distribution in time at $x = 0.05$ m, $x = 0.1$ m and $x = 0.15$ m for $M = 24 \times 1R_x2$ mesh using timesteps of $\Delta t = 0.50$ day and $\Delta t = 1.00$ day.

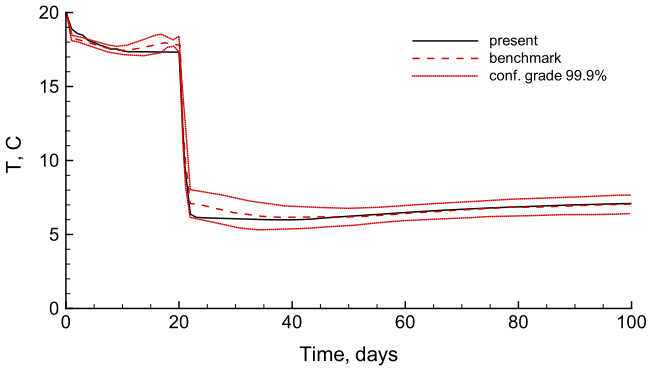

Fig. 6. Temperature distribution in time at $x = 0.05$ m. Comparison with [15,16] is shown.

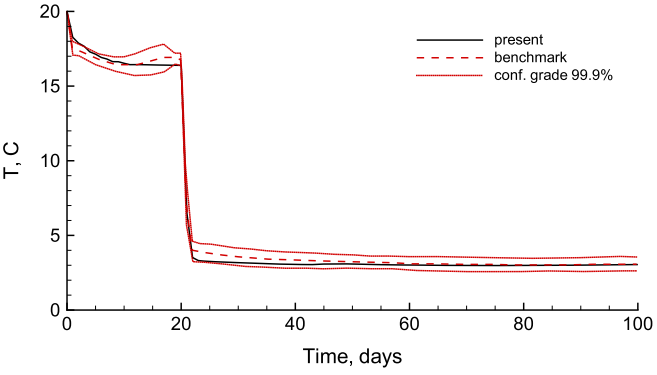

Fig. 7. Temperature distribution in time at $x = 0.1$ m. Comparison with [15,16] is shown.

$$\frac{\partial \varphi}{\partial n} = 0 \quad \text{and} \quad \frac{\partial T}{\partial n} = 0 \quad \text{for } t > 0. \tag{54}$$

The initial conditions were

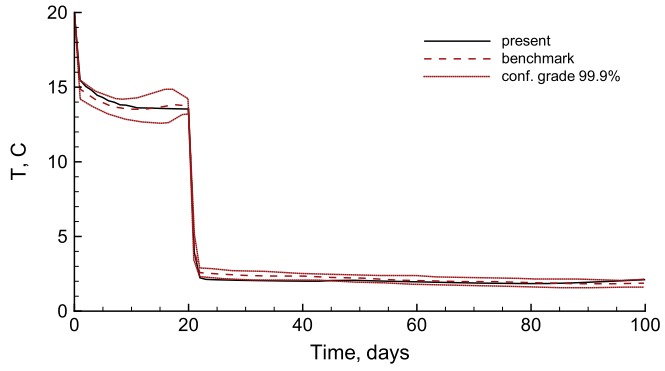

Fig. 8. Temperature distribution in time at $x = 0.15$ m. Comparison with [15,16] is shown.

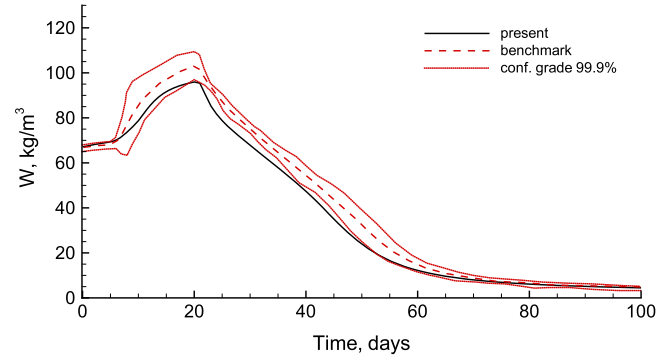

Fig. 9. Moisture distribution in time at $x = 0.05$ m. Comparison with [15,16] is shown.

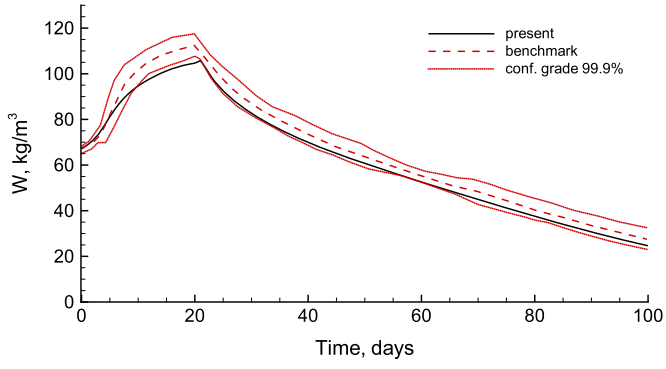

Fig. 10. Moisture distribution in time at $x = 0.1$ m. Comparison with [15,16] is shown.

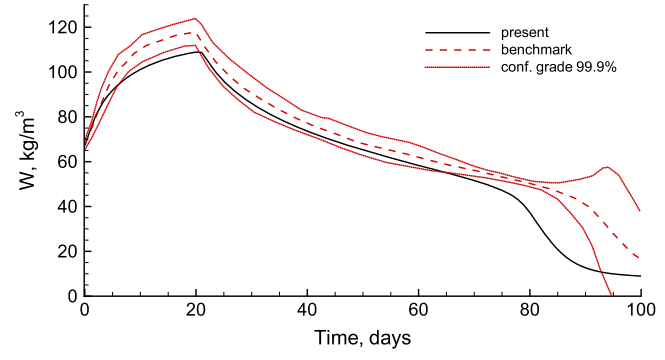

Fig. 11. Moisture distribution in time at $x = 0.15$ m. Comparison with [15,16] is shown.

$$\varphi_o = 0.95, \quad T_o = 20\ ^\circ\mathrm{C} \quad \text{and} \quad p_o = 1.0{\cdot}10^5\ \mathrm{Pa} \quad \text{at } t = 0. \tag{55}$$

All the relevant transport and material properties are given in Table 1 for the material (C). The sorption isotherm was given by the following expression:

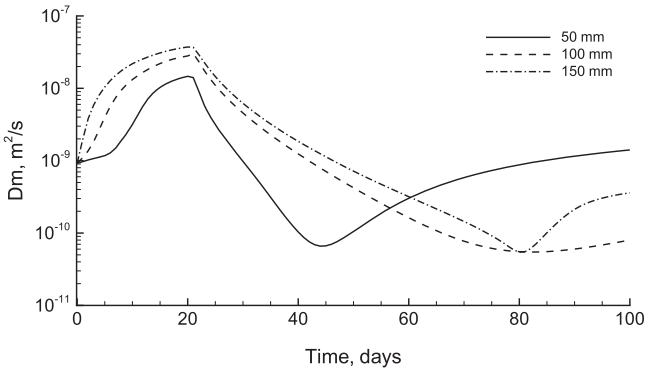

Fig. 12. Diffusivity distribution in time at $x = 0.05$ m, $x = 0.10$ m and $x = 0.15$ m.

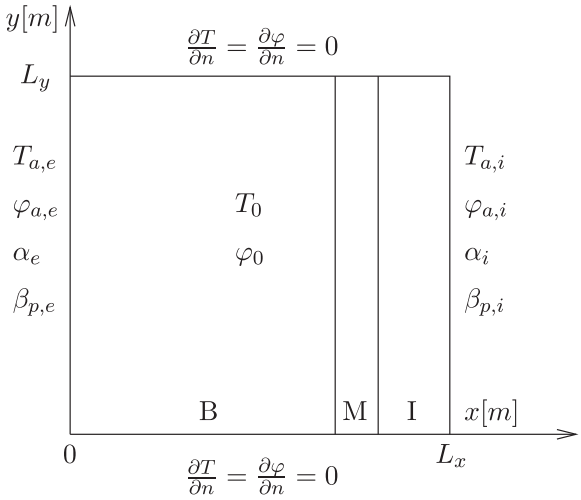

Fig. 13. Capillary-active inside insulation: outline of the structure, initial and boundary conditions: $L_x = 0.420$ m, $L_y = 0.001$ m, $\delta_b = 0.365$ m, $\delta_m = 0.015$ m, $\delta_i = 0.040$ m, simulation time 60 days.

$$W(\varphi) = W_{sat} \sum_{i=1}^{2} \frac{k_i}{[1 + (a_i h)^{n_i}]^{m_i}}, \qquad h = \frac{p_{suc}}{\rho_l g} = -\frac{R_w T \ln(\varphi)}{g}, \tag{56}$$

with the exponent $m_i = 1 - 1/n_i$. The vapor permeability δ_p and liquid water permeability D_l transport coefficients were given by the following expressions

$$\delta_p(W, T) = \frac{D_{va}}{\mu R_w T} \frac{1 - \dfrac{W}{W_{sat}}}{(1 - p)\left(1 - \dfrac{W}{W_{sat}}\right)^2 + p}, \tag{57}$$

$$D_l(W) = \exp\left[\sum_{i=0}^{5} a_i \left(\frac{W}{\rho_l}\right)^i\right]. \tag{58}$$

Effective thermal conductivity and specific heat per volume for dry material, respectively, were given by the following relationships:

$$\lambda_{eff} = \lambda_m + \lambda_{mst} \frac{W}{\rho_l} \quad \text{and} \quad c_m = c_{pm} \rho_m. \tag{59}$$

The air permeability δ_a and air properties $c_a = c_{pa}\rho_a$ were assumed to be constant

$$\delta_a = 7.5{\cdot}10^{-6}\,[\mathrm{s}] \quad \text{and} \quad c_{pa}\rho_a = 1000{\cdot}1.25 = c_a = 1.25{\cdot}10^3\ \mathrm{J/m^3\,K}. \tag{60}$$

The temperature and moisture distribution in time were examined to assess the numerical error related to the time step value. Fig. 5 presents time plots of temperature and moisture at three locations for different time steps. There are minor differences in the results which were observed at the beginning of the simulation. We conclude that the

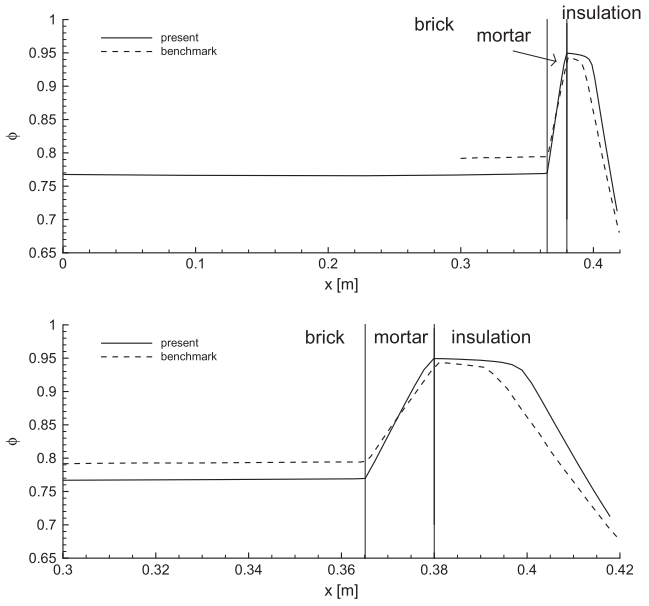

Fig. 14. Relative humidity profile of the inside insulation and the mortar layer after 60 days. Comparison with [15,16] is shown.

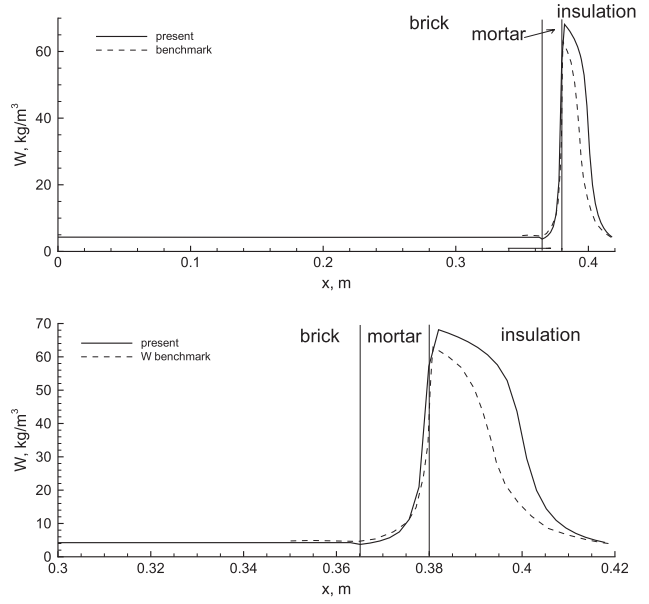

Fig. 15. Moisture content profile of the inside insulation and the mortar layer after 60 days. Comparison with [15,16] is shown.

mesh and the short time step are adequate and present these results in a further analysis. Time plots of temperature and moisture at three locations and comparison with the benchmark results are shown in Figs. 6–11. As these figures show, the BEM numerical simulation results agree well with the benchmark results [15,16].

This test case is more challenging as it involves different physical phenomena, such as redistribution of heat and moisture caused by diffusion and convection, inherent severe nonlinearity of the transport coefficients, and the system is exposed to realistic internal and external boundary conditions. Fig. 12 presents the time plot of the moisture diffusivity D_m at three locations. A marked variation of the moisture diffusivity can clearly be seen for a few orders of magnitude. Because of this aspect, the variation of the Peclet cell number value, i.e. defined as $Pe_{cell} = v{\cdot}L_x/M/D_m$, lies in the range of $Pe_{cell} \approx 1.5{\cdot}10^2 - 1.5{\cdot}10^5$, whilst $Pe_{cell} \approx 8.5{\cdot}10^3$ for the initial hygrothermal conditions.

5.3. Moisture redistribution inside capillary-active interior insulation

The benchmark test example [15,16] deals with the moisture redistribution inside an inhomogeneous multilayered wall $L_x = 0.420$ m thick and $L_y = 0.001$ m tall with capillary-active interior insulation. The wall consists of three layers: brick (A) $\delta_b = 0.365$ m, mortar (B) $\delta_m = 0.015$ m and insulating material (C) $\delta_i = 0.040$ m, shown in Fig. 13, The multilayered structure is airtight. Thermal conductivity of the brick and the insulating material differs by a factor of 11 in dry conditions. Initial temperature and relative humidity conditions are both constant for the entire wall. At time zero there is a sudden change in temperature and vapor pressure on either side of the wall. The simulation time is 60 days.

The following boundary conditions of the third kind could be prescribed on the left boundary at $x = 0$ m and $0 \le y \le L_y$:

$$T_{a,e} = 0.0\ ^\circ\text{C} \quad \text{and} \quad \alpha_e = 25.00\ \text{W/m}^2\,\text{K} \quad \text{for } t > 0 \varphi_{a,e} = 0.8 \quad \text{and} \quad \beta_{p,e} = 1.8382{\cdot}10^{-7}\ \text{s/m} \quad \text{for } t > 0, \tag{61}$$

on the right boundary at $x = L_x$ and $0 \le y \le L_y$

$$T_{a,i} = 20.0\ ^\circ\text{C} \quad \text{and} \quad \alpha_i = 8.00\ \text{W/m}^2\,\text{K} \quad \text{for } t > 0 \varphi_{a,i} = 0.6 \quad \text{and} \quad \beta_{p,i} = 5.8823{\cdot}10^{-8}\ \text{s/m} \quad \text{for } t > 0, \tag{62}$$

and zero Neumann boundary conditions were prescribed elsewhere:

$$\frac{\partial \varphi}{\partial n} = 0 \quad \text{and} \quad \frac{\partial T}{\partial n} = 0 \quad \text{for} \quad t > 0. \tag{63}$$

The initial hygrothermal conditions of the structure were

$$\varphi_o = 0.95 \quad \text{and} \quad T_o = 25\ ^\circ\text{C} \quad \text{at } t = 0 \tag{64}$$

throughout the whole construction.

All the transport and materials properties for all three layers are taken from [15] and are given by the following expressions. The sorption isotherms were given by the following expression:

$$W(\varphi) = W_{sat} \sum_{i=1}^{2} \frac{k_i}{[1 + (a_i h)^{n_i}]^{m_i}}, \quad h = \frac{p_{suc}}{\rho_l g} = -\frac{R_w T \ln(\varphi)}{g}, \tag{65}$$

with the exponent $m_i = 1 - 1/n_i$. The expressions for vapor permeability δ_P and liquid water permeability D_l transport coefficients were given by the following expressions:

$$\delta_p(W, T) = \frac{D_{va}}{\mu R_w T} \frac{1 - \dfrac{W}{W_{sat}}}{(1 - p)\left(1 - \dfrac{W}{W_{sat}}\right)^2 + p}, \tag{66}$$

$$D_l(W) = \exp\left[\sum_{i=0}^{5} a_i \left(\frac{W}{\rho_l}\right)^i\right], \tag{67}$$

and the relations for the effective thermal conductivity and specific heat per volume for dry material, respectively, were given by the following relationships:

$$\lambda_{eff} = \lambda_m + \lambda_{mst} \frac{W}{\rho_l} \quad \text{and} \quad c_{pm}\rho_m = c_m. \tag{68}$$

Corresponding material properties for each single layer are summarized in Table 1.

A uniform mesh of $M = 840 \times 1$ macro-elements was used. The convergence criterion used was $\epsilon = 10^{-8}$, and the under-relaxation parameter was set to ur=0.8. Time dependent analysis was performed by running the simulation from the initial state with a time step value of $\Delta t = 360.0$, $\Delta t = 3600.0$ and $\Delta t = 36\,000.0$ s. The purpose was to calculate the moisture distribution after t=60 day.

The relative humidity and moisture distribution between the inside insulation and the mortar layer after 60 days are shown in Figs. 14 and 15. The solution results of this three layered structure for all three time

step values closely match each other and the benchmark results.

6. Conclusions

The boundary element method has been formulated and implemented to solve the two-dimensional time-dependent coupled nonlinear heat, moisture and air flow through a porous solid. Quadratic basis functions were used to approximate the field functions and constant interpolation for fluxes, and the linear variation of all functions over each individual time step was assumed.

Three one-dimensional benchmarks consisting of moisture uptake in a semi-infinite region, air transfer through a lightweight wall, and moisture redistribution inside a multilayered wall with capillary-active interior insulation, were analyzed. The simulations accounted for very complicated coupled nonlinear processes. The numerical iterative solution of each problem is therefore very demanding for several reasons: the time and length scales of the individual transport processes are very different, accurate modeling of diffusion and convection is required, transport properties are functions of the driving potentials, and boundary conditions of the third kind and the interface conditions introduce additional severe nonlinearities. The good agreement obtained with the test cases suggests that the simulation model based on a BEM numerical technique can be used to simulate the hygrothermal performance of building envelope components.

Acknowledgments

The research work presented herein was supported by the projects POCI-01-0145-FEDER-016852 (GRLF) and POCI-01-0247-FEDER-003393 (green URBANLIVING), founded by Portugal 2020 through the Operational Programme for Competitiveness Factors (COMPETE 2020).

References

[1] Hagentoft CE. Introduction to building physics. Lund: Studentlitteratur; 2001.
[2] Tariku F, Kumaran K, Fazio P. Transient model for coupled heat, air and moisture transfer through multilayered porous media. Int J Heat Mass Transf 2010;53:3035–44.
[3] European standard (EN 15026:2007): hygrothermal performance of building components and building elements – assessment of moisture transfer by numerical simulation; 2007. p. 1–24.
[5] Ramšak M, Škerget L. A subdomain boundary element method for high-Reynolds laminar flow using stream function-vorticity formulation. Int J Numer Methods 2004;46:815–47.
[6] Škerget L, Brebbia CA. Progress in boundary element methods, In: Time dependent non-linear potential problems, vol. 3. Berlin, Heidelberg, New York: Springer-Verlag; 1984. [Chapter 3].
[7] Popov V, Power H, Škerget L. Domain decomposition techniques for boundary elements, application to fluid flow. In: Advances in boundary element series. Southampton, Boston: WIT Press; 2007.
[8] Wrobel LC. The boundary element method. Applications in thermo-fluids and acoustics, vol. 1. New York: John Wiley & Sons Ltd; 2002.
[9] Brebbia CA. The boundary element method for engineers. London: Pentech Press; 1978.
[11] Hagentoft CE, Kalagasidis AS, Adl-Zarrabi B, Roels S, Carmeliet J, Hens H, et al. Assessment method of numerical prediction models for combined heat, air and moisture transfer in building components. Benchmarks for one-dimensional cases. Report.
[12] Ramšak M, Škerget L, Hriberšek M, Žunič Z. A multidomain boundary element method for unsteady laminar flow using stream function vorticity equations. Eng Anal Bound Elem 2005;29:1–14.
[13] Ramšak M, Škerget L. A multidomain boundary element method for two equation turbulence models. Eng Anal Bound Elem 2005;29:1086–103.
[14] Škerget L, Tadeu A. BEM numerical simulation of coupled heat and moisture flow through a porous solid. Eng Anal Bound Elem 2014;40:154–61.
[15] Hagentoft CE. HAMSTAD – final report: methodology of HAM-modeling. Report R-02:8. Gothenburg, Department of Building Physics, Chalmers University of Technology; 2002.
[16] Cornick S. Results of the HAMSTAD benchmarking exercises using hyglRC 1-D version 1.1. Research report IRC-RR-222. National Research Council of Canada; 2006.